Supporting Material

Low-temperature mineral engineering stabilizes anchored cobalt sites for ultrafast antibiotic destruction via electron transfer-driven radical/nonradical synergy

Liyao Ren[a], Ran Liu[a], Runbin Zeng[a], Lingling Cao[a], Wenyu Wang[b], Xuguang Li[a], Xing Xu[c], Yanxia Zhao[a], Liangguo Yan[a], Yanfei Li[a], Wen Song[a,] *

[a] School of Water Conservancy and Environment, University of Jinan, Jinan 250022, People's Republic of China

[b] School of Environmental Science and Engineering, Qilu University of Technology, Shandong Academy of Sciences, Jinan 250353, People's Republic of China

[c] Shandong Key Laboratory of Water Pollution Control and Resource Reuse, School of Environmental Science and Engineering, Shandong University, Qingdao 266237, Shandong, People's Republic of China

* Corresponding author

e-mail: stu_songw@ujn.edu.cn (W. Song)

CONTENTS

Text S1 Chemical reagents

Text S2 Catalyst characterization method

Text S3 First-order kinetic model

Text S4 Determination of the PMS decomposition efficiency

Text S5 Half-wave potentials calculation

Text S6 Quenching experiments

Text S7 Galvanic oxidation system

Text S8 Electrochemical impedance spectroscopy (EIS)

Text S9 Open circuit potential (OCP)

Text S10 DFT calculation

Table S1 Input materials and energy required to treat 1 ton TC wastewater through different systems

Table S2 The peak positions and peak areas of XPS.

Table S3 The specific surface area, mesopore volume and average pore diameter of ATP and Co-ATP

Table S4 The physicochemical properties of all pollutants

Table S5 Summary of descriptors data for pollutants

Table S6 The Fukui index of TC

Figure S1 The FTIR patterns of Co-ATP

Figure S2 XPS spectra of C 1s of Co-ATP before and after reaction

Figure S3 SEM images of (a) ATP, (b) 0:50 Co-ATP

Figure S4 TEM images of (a) ATP and (b-g) Elemental distribution map of EDS

Figure S5 Hysteresis curve of (a) ATP and (b) Co-ATP

Figure S6 The specific surface area, mesopore volume and average pore diameter of ATP and Co-ATP

Figure S7 The k_{obs} values of different TC degradation systems

Figure S8 Correlation between the PMS decomposition efficiency and the degradation efficiency

Figure S9 The impact of Cu^{2+}, Pb^{2+} and bovine serum albumin on the Co-ATP/PMS/TC system

Figure S10 The ultraviolet spectrum of DPA-$^1O_2$

Figure S11 The three-dimensional fluorescence spectrum of TC

Figure S12 The chemical structure of TC

Figure S13 The mass spectrum of the degradation pathway of TC

Figure S14 Toxicity analysis of TC degradation intermediate products:

(a) fathead minnow LC_{50} (96 hr) and bioaccumulation factor; (b) developmental toxicity; (c) mutagenicity.

Text S1 Chemical reagents

The reagents superoxide dismutase (SOD) was purchased from Shanghai Macklin Co., Ltd. (Shanghai, China). Tertbutyl alcohol (TBA) was bought from Sinopharm Chemical Reagent Co., Ltd. (Shanghai, China).

The deionized water was used for all solution preparations. Sodium hydroxide (NaOH) and hydrochloric acid (HCl) were obtained from Damao Chemical Reagent Co., Ltd. (Tianjin, China). Ethyl alcohol (EtOH) was acquired from Tianjin Fuyu Fine Chemical Co., Ltd. (Tianjin, China). Additionally, sodium chloride (NaCl), sodium nitrate ($NaNO_3$), and sodium sulfate (Na_2SO_4) were sourced from Tianjin Guangcheng Chemical Reagent Co., Ltd. (Tianjin, China). Sodium bicarbonate ($NaHCO_3$) was bought from Tianjin Hengxing Chemical Reagent Manufacturing Co., Ltd. (Tianjin, China).

Text S2 Catalyst characterization method

The following advanced characterization techniques were employed in this study: scanning electron microscope (SEM, Gemini 300, ZEISS Corporation, Germany), X-ray diffraction (XRD, Bruker D8-Advance diffractometer, Bruker Corporation, Germany), X-ray photoelectron spectroscopy (XPS, Thermo Escalab 250Xi, ThermoFisher Scientific, United States), the FTIR spectrometer (Thermo Scientific Nicolet iS5, ThermoFisher, United States), and electron paramagnetic resonance (EPR, Bruker A300, Bruker Corporation, Germany). The UV-visible spectrometer (UV5100, Shanghai) was employed to determine the concentration of pollutants.

Text S3 First-order kinetic model

The degradation curve of pollutants was fitted by reaction kinetics, which conforms to the first-order kinetic model. The first-order kinetic model was calculated by Eq. S1

$$\ln\left(\frac{C_t}{C_0}\right) = -k_{obs} \times t \qquad \text{(S1)}$$

In the formula, C_0 and C_t (mg/L) represent the initial and final concentrations of OTC, k_{obs} (min^{-1}) is the first-order reaction rate constant, t (min) is the reaction time.

Text S4 Determination of the PMS decomposition efficiency

To determine the PMS adsorption capacity of Co-ATP, 10 mg of materials was added into 100 mL deionized water. At predetermined time intervals, the suspension was withdrawn and filtered using a 0.45 μm filter membrane. The concentration of residual PMS was analyzed by a chromogenic method using N, N-diethyl-p-phenylenediamine sulfate (NDPDAS) as chromogenic agent. Typically, 0.2 mL sample aliquot was added to a mixed solution (1 mL of 40 mM $FeSO_4$, 0.4 mL of 100 mM NDPDAS, 8.4 mL of deionized water at pH 3.0) and shaken promptly for developing. The absorbance was measured at $\lambda_{absorption}$= 510 nm using an UV-vis spectrophotometer.

The PMS adsorption capacity (q_e) was obtained via a pseudo first order model:

$$\ln(q_e - q_t) = \ln q_e - k_1 t \quad \text{(S2)}$$

where q_e is adsorption capacity at equilibrium (mmol/g), q_t is absorbed amount of PMS at time t (mmol/g), and k_1 is the pseudo first order rate constant (min^{-1}).

Text S5 Half-wave potentials calculation

The CV tests were performed in an electrochemical workstation (CHI 660E). The experimental setup comprised a three-electrode system: a glassy carbon electrode as the working electrode, a platinum wire as the counter electrode, and an Ag/AgCl electrode as the reference electrode. The measurements were carried out in 50 mM Na_2SO_4 electrolyte containing 0.5 mM of the pollutants. The potential was swept between -0.1 V and +1.0~1.5 V at a scan rate of 10 mV. To ensure the reliability and comparability of the data, all experimental conditions, including pH, temperature and pollutants concentration, were meticulously controlled and held constant throughout the experiments.

Half-wave potentials ($\varphi_{1/2}$) were calculated by Eq. S3.

$$\varphi_{1/2} = \frac{1}{2}\left(E_p + E_{p/2}\right) \quad \text{(S3)}$$

where E_p and $E_{p/2}$ are the peak potential and half-peak potential (potential of half the peak current), respectively.

Text S6 Quenching experiments

The types of free radicals generated during the reaction were analyzed through quenching experiments and electron paramagnetic resonance analysis. At room temperature, 100 mL of an antibiotic pollutant solution with a free radical quenching agent at a concentration of 10 mg·L^{-1} was placed in a conical flask. The types and concentrations of the free radical quenchers were hydrogen peroxidase, 10 mmol L^{-1} tert-butanol, 0 mmol L^{-1} p-benzoquinone, 500 mmol L^{-1} ethanol, and 10 mmol L^{-1} TEMP. Then, a certain amount of catalyst was added to the solution in the conical flask and stirred on a magnetic stirrer. 1 mL of 0.1 mol L^{-1} PMS solution was added to start the free radical quenching experiment. Samples of 2 mL were taken at 0-30 minutes and the absorbance was measured.

Text S7 Galvanic oxidation system

For the preparation of platinum electrode coated with Co-ATP, 5 milligrams of Co-ATP was dispersed in 1 milliliter of ethanol solution containing 5% weight of Nafion perfluoropolymer resin. The mixture was stirred and subjected to 30 minutes of ultrasonic treatment. Subsequently, the resulting suspension was applied onto the platinum electrode and dried under an infrared oven. 100 ml of TC (10 mg/L) and PMS (1 mmol/L) solutions were placed in different beakers, with a salt bridge in between, and an ammeter was connected externally. The degradation experiment began, and 2 mL of samples were taken at times 0, 1, 2, 4, 6, 8, 10, 20, and 30, and filtered through a 0.45 μm PES membrane. The absorbance of the samples was measured using a UV spectrophotometer (UV-5100, Shanghai Yuanxie) with a wavelength of 314 nm.

Text S8 Electrochemical impedance spectroscopy (EIS)

To prepare the Co-ATP-coated glass carbon electrode (Co-ATP/GCE), 5 milligrams of Co-ATP was dissolved in 1 milliliter of N, N-dimethylformamide (DMF) solution containing 5% (by weight) Nafion perfluoropolymer. The mixture was stirred and subjected to 30 minutes of ultrasonic treatment. Subsequently, the resulting suspension was dropped onto the GCE and evenly coated and dried under an infrared oven. The prepared Co-ATP/GCE was then immersed in a 50 millimolar sodium sulfate solution overnight to stabilize the potential, followed by electrochemical analysis. The same method was used to prepare ATP/GCE.

Text S9 Open circuit potential (OCP)

The open circuit potential (OCP) refers to the electrode potential when the current density is zero. In electrochemical experiments, selecting the appropriate voltage setting is crucial, as OCP helps in precisely defining the intervals for strong, weak, and linear polarization. The OCP value is influenced by factors such as electrode material, electrolyte concentration, and temperature, but it remains unaffected by the external circuit. Monitoring changes in OCP during the experiment allows us to understand the voltage variations when PMS and pollutants are added to the electrolyte solution, thereby providing insights into the electron transport capabilities.

For the preparation of the Co-ATP-coated glassy carbon electrode (Co-ATP/GCE), 5 mg of Co-ATP was dispersed in 1 mL of N, N-dimethylformamide (DMF) solution containing 5 wt% Nafion perfluorinated resin. The mixture was stirred and subjected to ultrasonication for 30 minutes. Subsequently, the resulting suspension was drop-cast onto a GCE and dried in an oven at 60°C for 10 minutes. This drop-casting process was repeated three times to ensure uniform coating.

The prepared Co-ATP/GCE was then immersed in 50 mM Na_2SO_4 solution overnight to stabilize the potential before conducting electrochemical analyses. During the analysis, a saturated silver chloride electrode was used as a reference electrode to monitor the open-circuit potential changes upon the addition of peroxymonosulfate (PMS) and various pollutants (such as ciprofloxacin (CPFX), norfloxacin (NFX), ofloxacin (OFX), oxytetracycline (OTC), and tetracycline (TCH)).

The specific monitoring procedure was as follows: at 500 s, 1 mL of PMS (with a mother liquor concentration 0.1 M) was added to the electrolyte (assuming a 100 mL system), and the voltage change was recorded. At 2600 s, 5 mL of pollutants solution (with a mother liquor concentration 0.2 g/L) was added, and the voltage change was monitored until 3600 s.

Text S10 DFT calculation

The molecular configurations employed in this study were constructed using GaussView 5.0 and optimized via density functional theory (DFT) methods. The optimization was performed at the B3LYP-D3/6-31+G(d,p) level, incorporating solvation effects with water. Subsequent energy calculations for the optimized models, including density of states and adsorption energy, were carried out at the B3LYP-D3/6-311+G(d,p) level. All energy units were consistently expressed in electron volts (eV). Computational analyses were conducted using the Gaussian 09 software package. To ensure the stability of the optimized structures, vibrational frequency analysis was performed, confirming the absence of imaginary frequencies.

Table S1 Input materials and energy required to treat 1 ton TC wastewater through different systems

Treatment of 1 ton of Tetracycline wastewater （5 mg/L）	Homogeneous PMS system	Heterogeneous commercial Fe_3O_4 +PMS system	Heterogeneous Co-ATP+PMS system
Reagents (g)			
$FeSO_4·7H_2O$	2500	0	0
H_2SO_4	767	767	0
$NaSO_4$	7000	0	0
NaOH	400	400	0
Polyacrylamide	278	0	0
Fe_3O_4	0	1000	0
Potassium permonosulfate	512	256	56
Attapulgite	0	0	134
$Co(Ac)_2$	0	0	14
Power supply	2	0.4	0
Pumps (Fenton reactor)	1.6	0.8	0.8
Stirrer	2.4	2.4	2.8
Stirrer (reagents for the sludge treatment)	0.4	0	0
Pumps (reagents for the sludge treatment)	1.2	0	0
Chamber filter press	0.2	0	0
Heat for catalyst preparation	0	0	0.3

Outputs streams(g)			
Generated sludge, dry base	200	0	0
Exhausted catalyst	0	500	100

Table S2 The peak positions and peak areas of XPS

Element	Valence state	Peak Position		Area	
		before	after	before	after
Co $2P_{1/2}$	satellite	803.039	804.012	25467.490	18102.230
	Co^{2+}	797.834	798.516	15573.520	8554.198
	Co^{3+}	796.549	797.199	15573.520	11719.680
Co $2P_{3/2}$	satellite	786.493	786.889	36904.750	26445.920
	Co^{2+}	782.300	782.659	38628.510	26376.290
	Co^{3+}	780.753	781.212	44304.310	18768.710
Si	SiO_2	103.139	103.008	16353.000	40981.80
	SiO_x	102.474	103.451	15303.940	40576.050
C	C-O	284.475	284.686	8324.181	27799.420
	C-C	285.318	285.408	6407.081	23961.070
	C=C	286.602	286.750	5517.202	9942.709

Table S3 The specific surface area, mesopore volume and average pore diameter of ATP and Co-ATP

Sample	**S_{BET}(m^2/g)**	**V_{mic}(m^2/g)**	**D_{Avg}（nm）**
ATP	34.68	10.55	5.34
Co-ATP	38.06	8.72	6.67

Table S4 The physicochemical properties of all pollutants

Chemical name	Structure	Molecular Formula	CAS
Tetracycline Hydrochloride (TC)	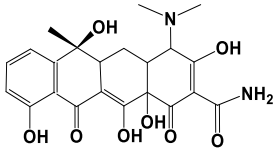	$C_{22}H_{24}N_2O_8 \cdot HCl$	64-75-5
Oxytetracycline (OTC)	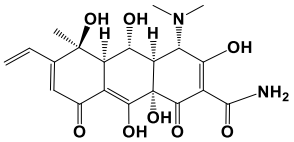	$C_{22}H_{24}N_2O_9$	79-57-2
Ofloxacin (OFX)	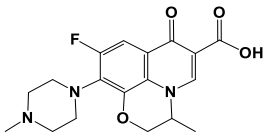	$C_{18}H_{20}FN_3O_4$	82419-36-1
Norfloxacin (NFX)	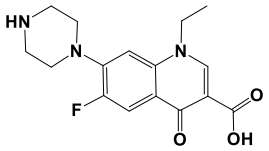	$C_{16}H_{18}FN_3O_3$	70458-96-7
Ciprofloxacin (CPFX)	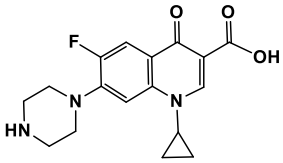	$C_{17}H_{18}FN_3O_3$	85721-33-1

Table S5 Summary of descriptors data for pollutants

Compound	E	N	$\varphi_{1/2}$	k_{obs}	lnk_{obs}	E_{HOMO} (eV)	E_{LUMO} (eV)
TC	1.5876	3.2399	0.946	0.9069	-0.0977	-5.8813	-2.7323
OTC	1.7612	3.1968	0.961	0.6362	-0.4522	-5.8864	-2.9399
OFX	0.9730	3.1890	1.267	0.1794	-0.9012	-5.9322	-1.6082
NFX	0.9726	3.0646	1.361	0.4061	-1.4881	-6.0566	-1.57363
CPFX	0.9693	3.0835	1.366	0.2258	-1.7181	-6.0377	-1.55785

Note:

E: Electrophilicity index; N: Nucleophilicity index

Table S6 The Fukui index of TC

Element	No.	q(n)	q(n-1)	q(n+1)	f^0	f^-	f^+
C	1	-0.19139	-0.11313	-0.13592	0.011395	0.07826	-0.05547
C	2	-0.29281	-0.06593	-0.14912	0.041595	0.22688	-0.14369
C	3	0.38485	0.25894	0.17049	0.044225	-0.12591	0.21436
C	4	-0.21722	-0.01189	-0.09484	0.041475	0.20533	-0.12238
C	5	-0.00154	-0.02303	-0.02386	0.000415	-0.02149	0.02232
C	6	-0.27777	0.02853	-0.13419	0.08136	0.3063	-0.14358
C	7	0.5281	0.2380	0.2033	0.0174	-0.2901	0.3249
C	8	-0.2176	0.0401	-0.1115	0.0758	0.2577	-0.1062
C	9	-0.2677	-0.1438	-0.1323	-0.0058	0.1239	-0.1355
C	10	0.2499	0.1289	0.1254	0.0017	-0.1210	0.1244
C	11	0.4318	0.2595	0.1747	0.0424	-0.1723	0.2572
C	12	0.1476	0.0718	0.0725	-0.0003	-0.0758	0.0751
C	13	-0.2916	-0.1467	-0.1475	0.0004	0.1448	-0.1441
C	14	-0.4579	-0.2305	-0.2269	-0.0018	0.2274	-0.2309
C	15	0.5518	0.2740	0.1074	0.0833	-0.2778	0.4445
C	16	-0.3050	-0.1468	-0.1172	-0.0148	0.1582	-0.1877
C	17	0.4625	0.2358	-0.0168	0.1263	-0.2267	0.4793
C	18	-0.1001	-0.0501	-0.0395	-0.0053	0.0500	-0.0606
O	19	-0.6999	-0.1953	-0.3655	0.0851	0.5047	-0.3344
O	20	-0.6070	-0.3008	-0.3591	0.0292	0.3062	-0.2479
O	21	-0.6580	-0.2454	-0.3461	0.0503	0.4126	-0.3119
O	22	-0.6145	-0.2931	-0.4301	0.0685	0.3214	-0.1844
O	23	-0.6259	-0.3054	-0.3681	0.0314	0.3205	-0.2578
C	24	0.6668	0.3274	0.3331	-0.0029	-0.3394	0.3337
N	25	-0.8542	-0.4100	-0.4361	0.0130	0.4442	-0.4182
O	26	-0.6149	-0.2483	-0.3248	0.0382	0.3666	-0.2901
N	27	-0.5708	-0.2858	-0.3021	0.0082	0.2850	-0.2687
C	28	-0.4719	-0.2376	-0.2341	-0.0017	0.2344	-0.2378
C	29	-0.4865	-0.2455	-0.2394	-0.0031	0.2409	-0.2471
C	30	-0.6963	-0.3517	-0.3478	-0.0020	0.3446	-0.3486
O	31	-0.7686	-0.3779	-0.3853	0.0037	0.3907	-0.3833

O	32	-0.7625	-0.3749	-0.4129	0.0190	0.3876	-0.3496
H	33	0.2445	0.1380	0.1148	0.0116	-0.1065	0.1298
H	34	0.25516	0.14027	0.1197	0.010285	-0.11489	0.13546
H	35	0.23502	0.12692	0.1116	0.00766	-0.1081	0.12342
H	36	0.26504	0.14877	0.12742	0.010675	-0.11627	0.13762
H	37	0.27158	0.13644	0.1342	0.00112	-0.13514	0.13738
H	38	0.26588	0.14019	0.125	0.007595	-0.12569	0.14088
H	39	0.24737	0.12811	0.11929	0.00441	-0.11926	0.12808
H	40	0.23454	0.12187	0.10374	0.009065	-0.11267	0.1308
H	41	0.53414	0.27053	0.2669	0.001815	-0.26361	0.26724
H	42	0.53358	0.27236	0.2679	0.00223	-0.26122	0.26568
H	43	0.51126	0.25899	0.24551	0.00674	-0.25227	0.26575
H	44	0.42678	0.21914	0.20222	0.00846	-0.20764	0.22456
H	45	0.44091	0.2204	0.22177	-0.000685	-0.22051	0.21914
H	46	0.24769	0.12895	0.11474	0.007105	-0.11874	0.13295
H	47	0.24457	0.11793	0.12059	-0.00133	-0.12664	0.12398
H	48	0.20841	0.10924	0.09643	0.006405	-0.09917	0.11198
H	49	0.2503	0.13007	0.11455	0.00776	-0.12023	0.13575
H	50	0.26045	0.12991	0.13436	-0.002225	-0.13054	0.12609
H	51	0.20586	0.10747	0.09672	0.005375	-0.09839	0.10914
H	52	0.24081	0.12562	0.11323	0.006195	-0.11519	0.12758
H	53	0.23928	0.12957	0.11817	0.0057	-0.10971	0.12111
H	54	0.25979	0.1292	0.1311	-0.00095	-0.13059	0.12869
H	55	0.49623	0.25177	0.24349	0.00414	-0.24446	0.25274
H	56	0.5091	0.25897	0.25067	0.00415	-0.25013	0.25843

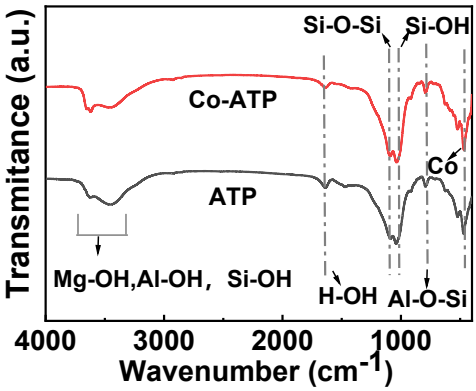

Figure S1 The FTIR patterns of Co-ATP

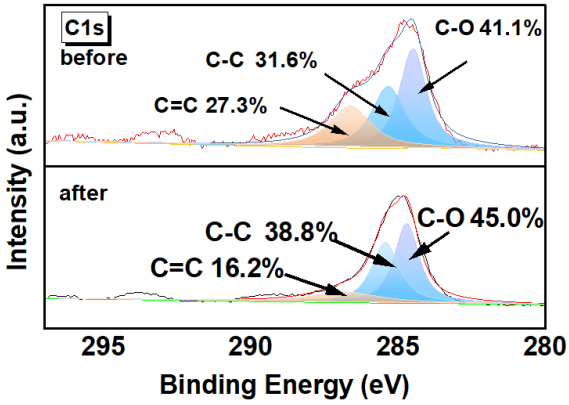

Figure S2 XPS spectra of C 1s of Co-ATP before and after reaction

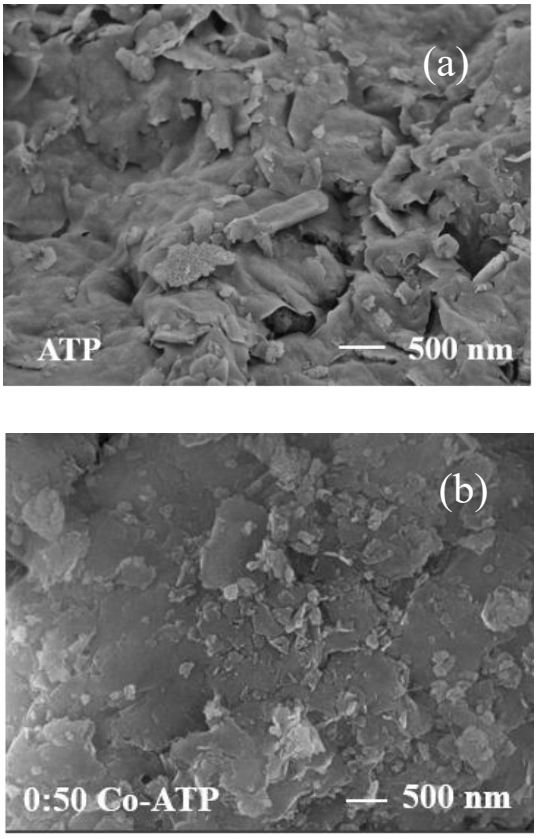

Figure S3 SEM images of (a) ATP, (b) 0:50 Co-ATP

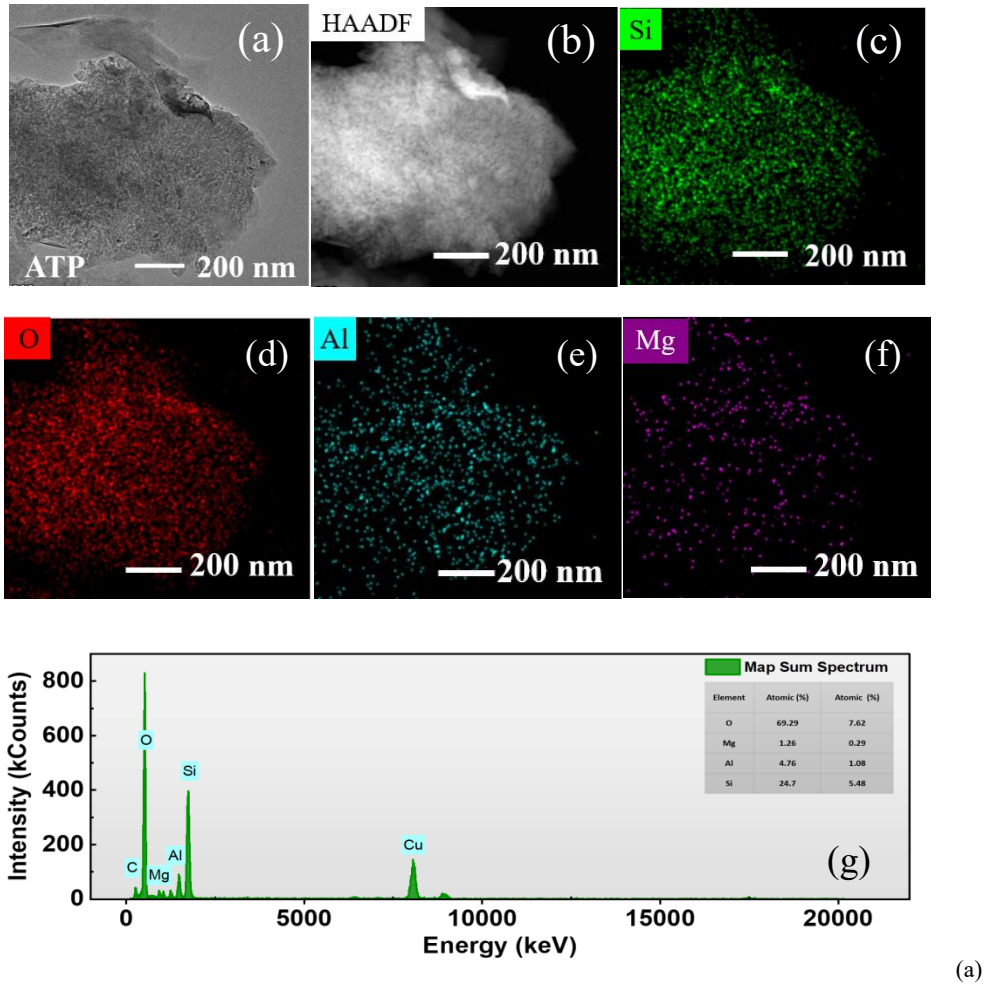

(a)

Figure S4 TEM images of (a) ATP and (b-g) Elemental distribution map of EDS

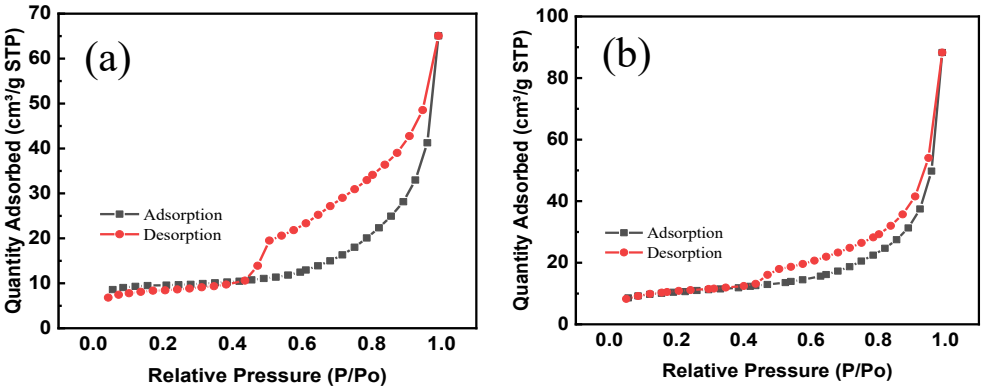

Figure S5 Hysteresis curve of (a) ATP and (b) Co-ATP

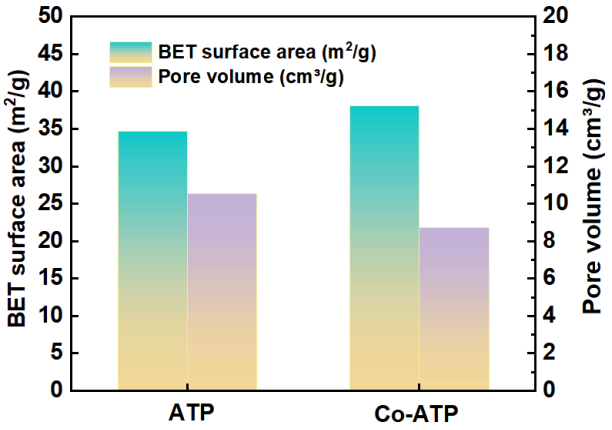

Figure S6 The specific surface area, mesopore volume and average pore diameter of ATP and Co-ATP

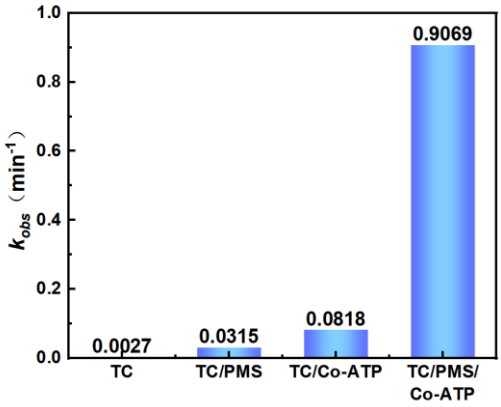

Figure S7 The k_{obs} values of different TC degradation systems

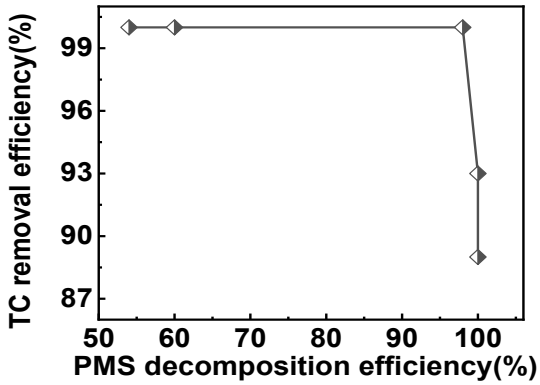

Figure S8 Correlation between the PMS decomposition efficiency and the degradation efficiency

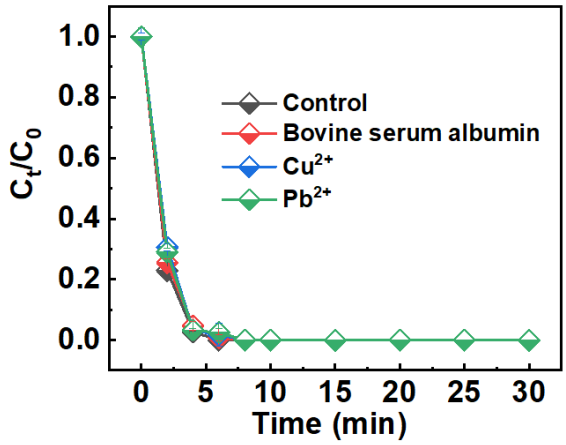

Figure S9 The impact of Cu^{2+}, Pb^{2+} and bovine serum albumin on the Co-ATP/PMS/TC system

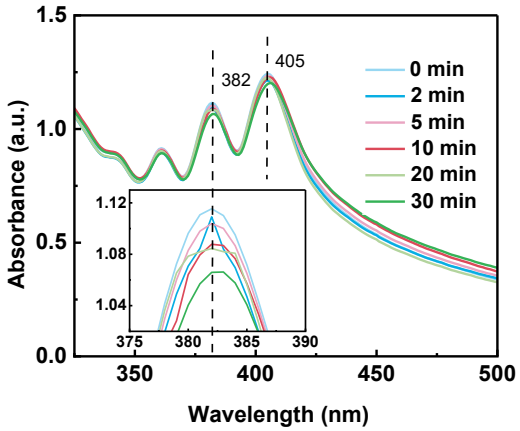

Figure S10 The ultraviolet spectrum of DPA-$^1O_2$

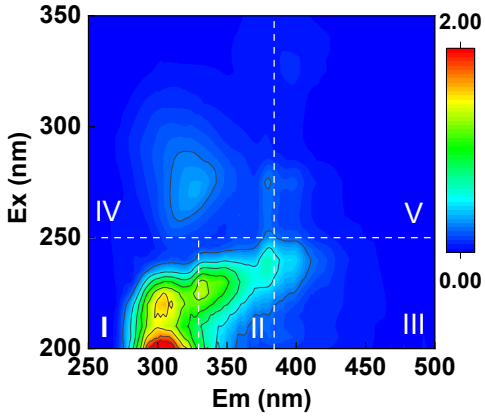

Figure S11 The three-dimensional fluorescence spectrum of TC

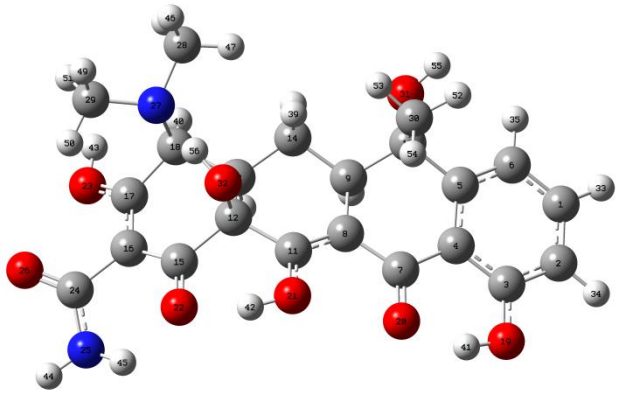

Figure S12 The chemical structure of TC

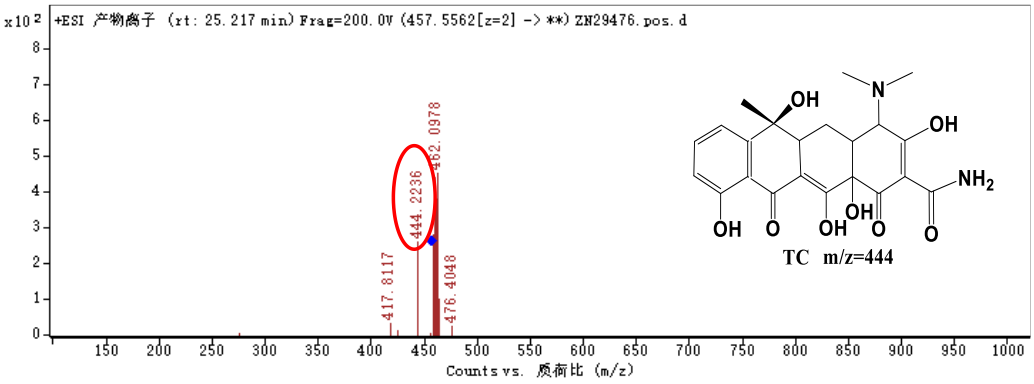
x10 2 +ESI 产物离子 (rt: 25.217 min) Frag=200.0V (457.5562[z=2] -> **) ZN29476.pos.d
462.0978
444.2236
417.8117
476.4048
Counts vs. 质荷比 (m/z)
TC m/z=444

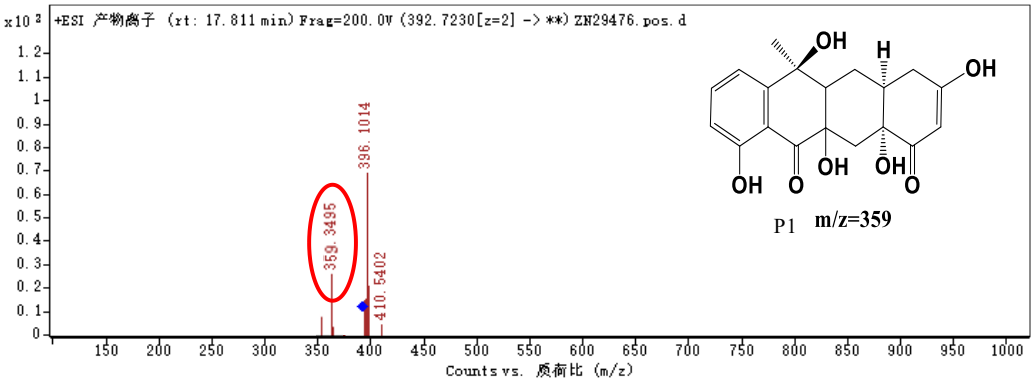
x10 3 +ESI 产物离子 (rt: 17.811 min) Frag=200.0V (392.7230[z=2] -> **) ZN29476.pos.d
386.1014
359.3495
410.5402
Counts vs. 质荷比 (m/z)
P1 m/z=359

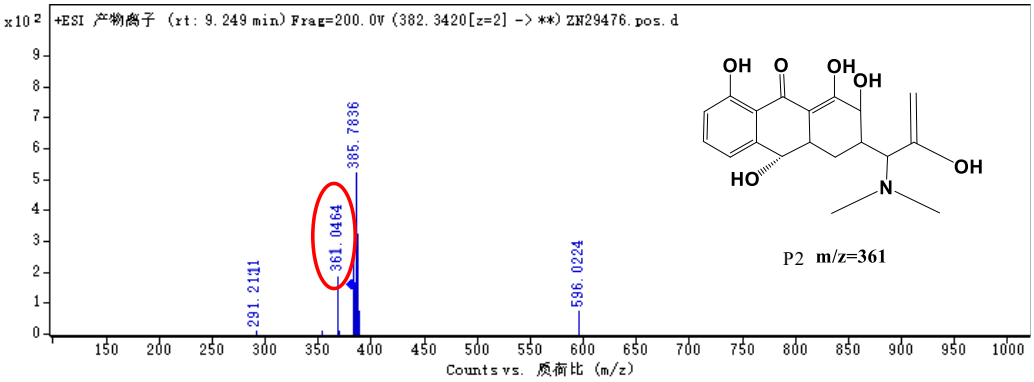
x10 2 +ESI 产物离子 (rt: 9.249 min) Frag=200.0V (382.3420[z=2] -> **) ZN29476.pos.d
385.7836
361.0464
291.2141
596.0224
Counts vs. 质荷比 (m/z)
P2 m/z=361

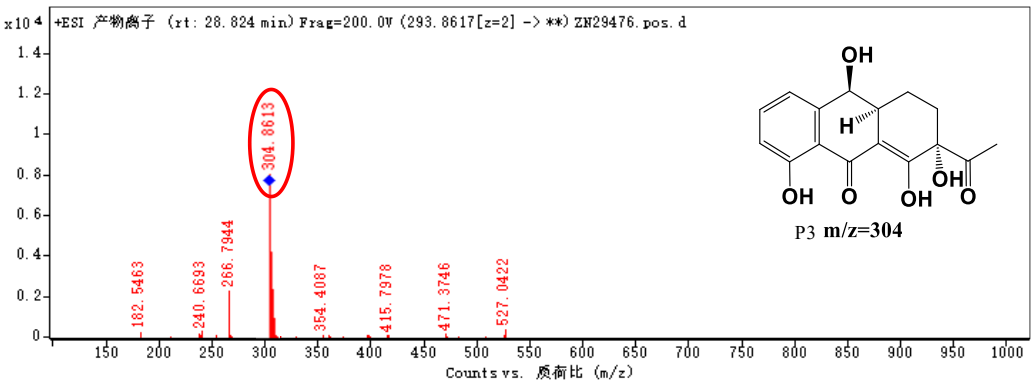
x10 4 +ESI 产物离子 (rt: 28.824 min) Frag=200.0V (293.8617[z=2] -> **) ZN29476.pos.d
304.8613
182.5463
240.6693
266.7944
354.4087
415.7978
471.3746
527.0422
Counts vs. 质荷比 (m/z)
P3 m/z=304

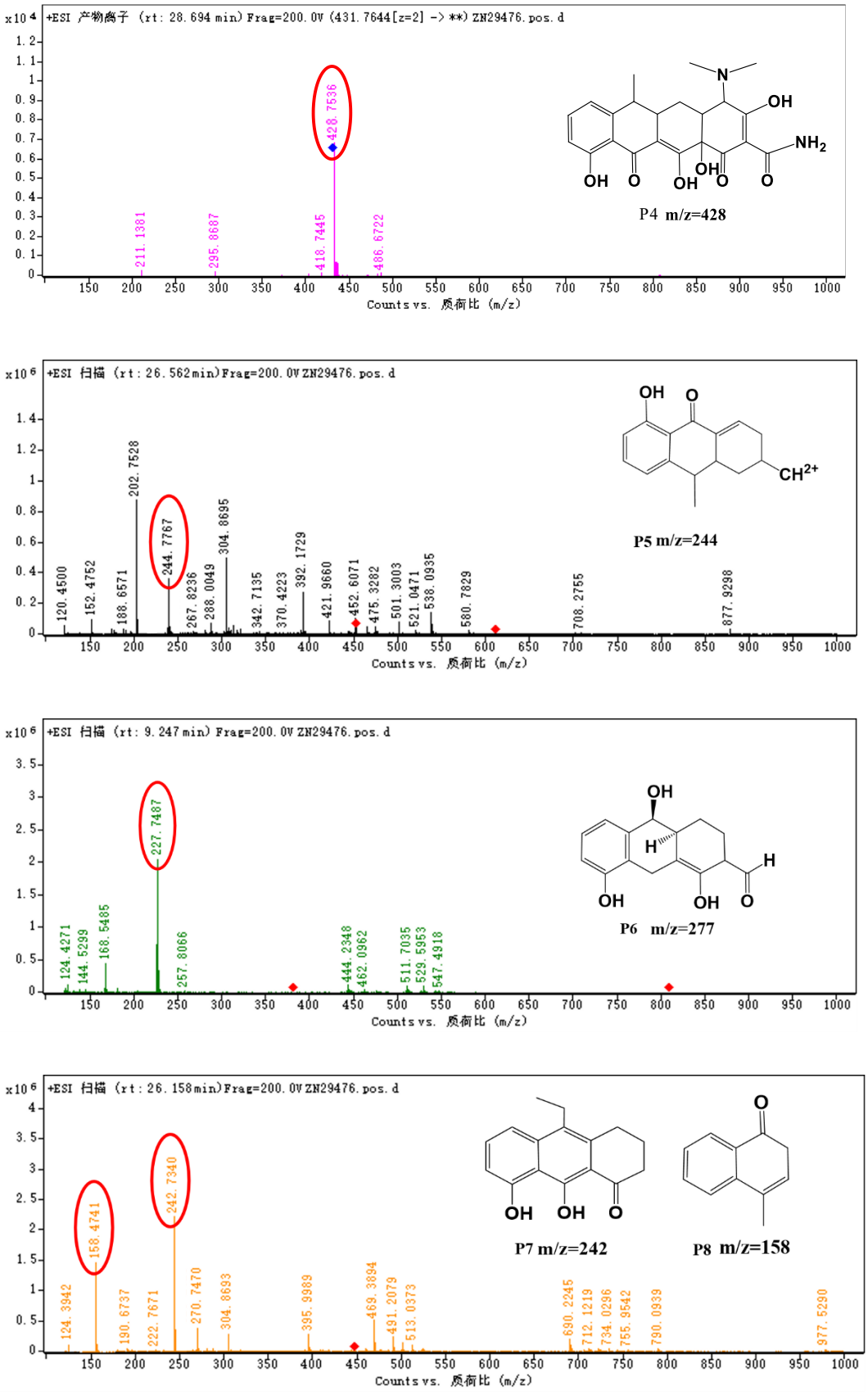

Figure S13 The mass spectrum of the degradation pathway of TC

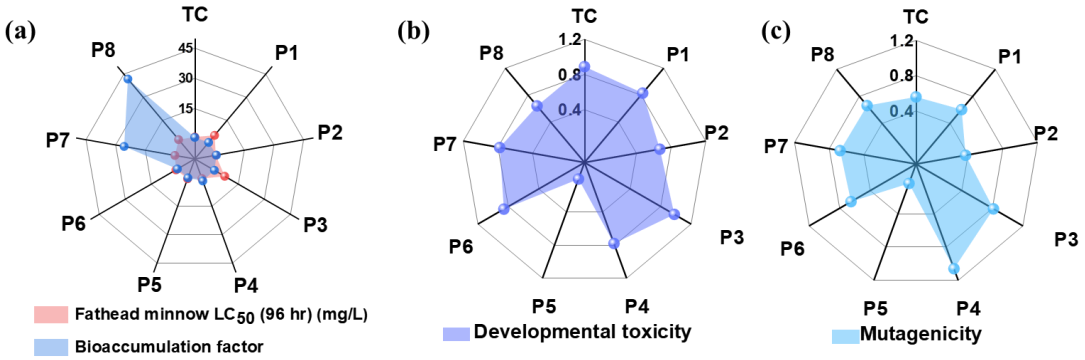

Figure S14 Toxicity analysis of TC degradation intermediate products: fathead minnow LC_{50} (96 hr) and bioaccumulation factor; (b) developmental toxicity; (c) mutagenicity.